임 종 훈 교수 지도

석사학위 청구논문

Copper Phosphide Enable the Selective Production of Reactive Oxygen Species

2024

성신여자대학교 대학원

미래응용과학학과

조 시 현

Copper Phosphide Enable the Selective Production of Reactive Oxygen Species

임 종 훈 교수 지도

이 논문을 석사학위논문으로 제출함

2024년 5월

성신여자대학교 대학원
미래응용과학학과
조 시 현

인 준 서

조시현의 석사학위 논문으로 인준함

2024년 7월

심사위원장 이 세 현 (서명 또는 인)

심 사 위 원 임 종 훈 (서명 또는 인)

심 사 위 원 원 승 현 (서명 또는 인)

성신여자대학교 대학원

Abstract

Copper Phosphide Enable the Selective Production of Reactive Oxygen Species

Jo, Si Hyeon
Department of Next Generation Applied Sciences
Graduate School of
Sungshin University

Copper phosphide (Cu_xP) has been previously reported to spontaneously generate hydroxyl radicals under certain reaction conditions (pH 3/dark), facilitating the degradation of aquatic pollutants. However, Cu_xP demonstrated reduced stability in acidic conditions, leading to a decrease in pollutant degradation efficiency upon repeated reactions. There has been a lack of research on the catalytic activity of Cu_xP under neutral conditions and the mechanisms behind such reactions.

Therefore, this study focused on maintaining reactivity while enhancing the stability of the Cu_xP in neutral conditions. To this end, Cu_xP served as an effective photocatalyst, demonstrated by its performance under visible light irradiation. Under the condition of pH 3/dark, strong acidity caused leaching of Cu and P elements into the

aqueous solution, gradually decreasing its reactivity with repeated degradation experiments. In contrast, under visible light irradiation at pH 7, the stability of the catalyst solution was maintained, resulting in consistent degradation efficiency across multiple pollution degradation experiments. Additionally, the reaction mechanisms, which vary according to each condition, were elucidated. The two systems showed different oxidation mechanisms while pollutants were degraded in a similar tendencies at pH 3/dark, degradation rates and efficiencies varied among pollutants at pH 7/visible. This variation is attributed to the different types of radicals generated in each systems. Experiments employing a range of radical scavengers and probes showed that, in the dark at pH 3, oxygen is reduced to hydroxyl radicals ($^{\bullet}OH$) through electron transfer pathway, showcasing significant oxidative strength. Conversely, under visible light at pH 7, singlet oxygen ($^{1}O_2$) formation occurred via an energy transfer mechanism. The generation of different types of radicals under each reaction condition was definitively proven through electron paramagnetic resonance (EPR) analysis. The unique properties of Cu_xP suggest a new strategy for the selective generation of reactive oxygen species (ROS) for the treatment of specific organic pollutants and pave the way for the development of advanced oxidation process systems (AOPs).

Key words: AOPs, Photocatalyst, Copper phosphide, Singlet oxygen, Hydroxyl radical

Contents

List of Figure Captions

Figure 8. A scheme depicting the generation of $^{\bullet}OH$ at pH 3 in the dark (left) and the production pathway of $^{1}O_2$ at pH 7 under visible light irradiation (right) through Cu_xP.

Figure 9. EPR spectra of (a) $^{\bullet}OH$-DMPO adducts at pH 3 ($[DMPO]_0$ = 90 mM), and $^{1}O_2$-TEMP adducts at pH 7 ($[TEMP]_0$ = 0.17 M) formed in Cu_xP suspeneion under dark or visible light irradiation ($[Cu_xP]_0$ = 1 g/L and air-equilibrated).

Figure 10. Reduction of diverse organic pollutants through Cu_xP (a) at dark/ pH 3 and (b) under visible light irradiation (λ > 420 nm)/ pH 7 ($[Cu_xP]_0$ = 1 g/L, [organic pollutants]$_0$ = 20 μM).

Figure 11. Assessment of FFA decomposition capability in the presence of (a) NOMs, (b) anions, and (c) in actual surface water and wastewater. The dark bars (left) were obtained at pH 3 in the dark, and the white bars (right) were obtained at pH 7 under visible light irradiation ($[Cu_xP]_0$ = 1 g/L, $[FFA]_0$ = 20 μM, [NOMs] = 10 ppm and [anion] = 10 mM).

Figure 12. *E. coli* inactivation dynamics in a Cu_xP suspension at pH 7, comparing dark with visible light exposure ($[Cu_xP]_0$ = 1 g/L and initial cell density = 107 cfu/mL).

Figure 13. FFA repeatedly decomposes FFA through Cu_xP at (a) pH 3/dark $[FFA]_0$ = 100 μM and (b) pH 7/visible light $[FFA]_0$ = 20 μM (c) amounts of Cu and P species leached from Cu_xP after reacting for 4 hours.

Figure 14. Cu_xP XPS analysis for (a) Cu 2p and (b) P 2p used and fresh and (c) Comparison of Cu_xP XRD patterns, after and before repeated

reaction at pH 7 under visible light.

Figure 15. The transformation in color of the Cu_xP suspension observed through multiple cycles of reaction, (a) dark at pH 3 and (b) under visible light at pH 7.

Ⅰ. Introduction

1. Photocatalyst

Photocatalyst utilizes the energy of light to accelerate chemical reactions. This technology is gaining attention as an eco-friendly approach because it employs solar energy without the need for additional electrical or chemical energy sources. Thanks to these advantages, photocatalyst can be applied in various fields such as the removal of Volatile Organic Compounds (VOC) [1-3] and aquatic pollutants [4-6], the generation of green hydrogen [7-10], and the CO_2 reduction [11-13].

Among the widely recognized photocatalysts are TiO_2, ZnO, CdS, WO_3, and graphitic carbon nitride (g-C_3N_4). These photocatalysts possess inherent bandgap energies, which are critical in determining their activation properties. Fig. 1 illustrates the bandgap energy levels of various photocatalysts. Since over 95% of solar energy comprises wavelengths longer than visible light, an ideal photocatalyst should be capable of activation in the visible light. The equation delineating the correlation between the bandgap energy of photocatalysts and photon energy is as follows (Eq. (1)) [14].

$$E_g = h\nu = \frac{hc}{\lambda} = \frac{1.2397 \times 10^3}{\lambda(nm)} \text{ [eV]} \quad (1)$$

Thus, the maximum bandgap size required for activation in the visible light region ($\lambda > 380$ nm) is 3.26 eV.

In photocatalytic materials, here the valence band (VB) embodies a

stabilized electron-rich state, and the conduction band (CB) represents a lower energy echelon with a paucity of electrons. The energy difference between these two bands is called the bandgap energy (E_g). Fig. 2 illustrates a schematic overview of the photocatalytic reaction. The reactions commence when the photocatalyst absorbs solar energy greater than its bandgap energy (E_g). (Eq. (2)) When electrons in the CB receive light energy exceeding the bandgap energy, they are excited to the VB, creating holes in the CB. These activated electrons and the generated holes move to the surface of the photocatalyst, inducing oxidation and reduction reactions. In the VB, H_2O is oxidized to produce reactive oxygen species (ROS) (Eq. (3)), while in the CB, O_2 is reduced to generate ROS (Eq. (4)). The produced ROS effectively decompose organic pollutants. However, the reaction ceases if the activated electrons recombine with the VB (Eq. (5)), so minimizing electron recombination and facilitating efficient electron transfer for continuous oxidation-reduction reactions is crucial [15].

$$\text{photocat.} + h_v \rightarrow e^- + h^+ \text{ (excitation)} \quad (2)$$

$$e^- + H_2O \rightarrow \text{ROS} \quad (3)$$

$$h^+ + O_2 \rightarrow \text{ROS} \quad (4)$$

$$4e^- + h^+ \rightarrow \text{recombination} \quad (5)$$

This study proposes a new photocatalytic-water treatment system utilizing the yet to be fully explored Cu_xP catalyst in the application of aquatic organic pollutant treatment. The system aims to achieve high

efficiency, stability, and cost-effectiveness. The system using the Cu_xP catalyst overcomes the limitations of existing photocatalysts and presents the possibility of activation across a broader wavelength range. Moreover, this new photocatalyst, being less toxic and economically advantageous, suggests its applicability in the field of water treatment.

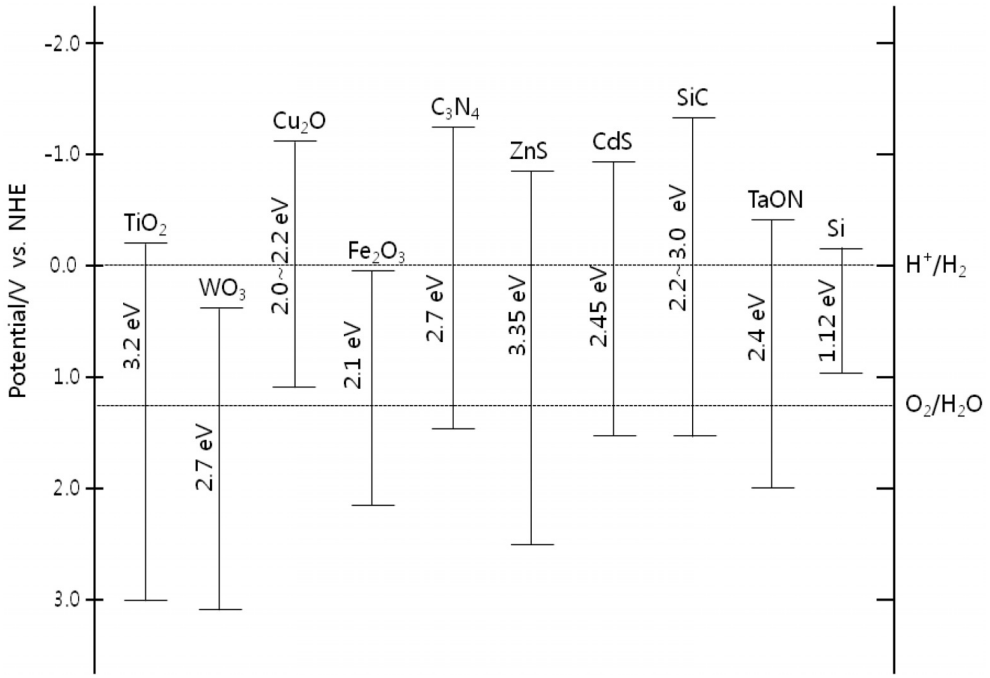

Figure. 1 Band gap energy level and size of various photocatalysts

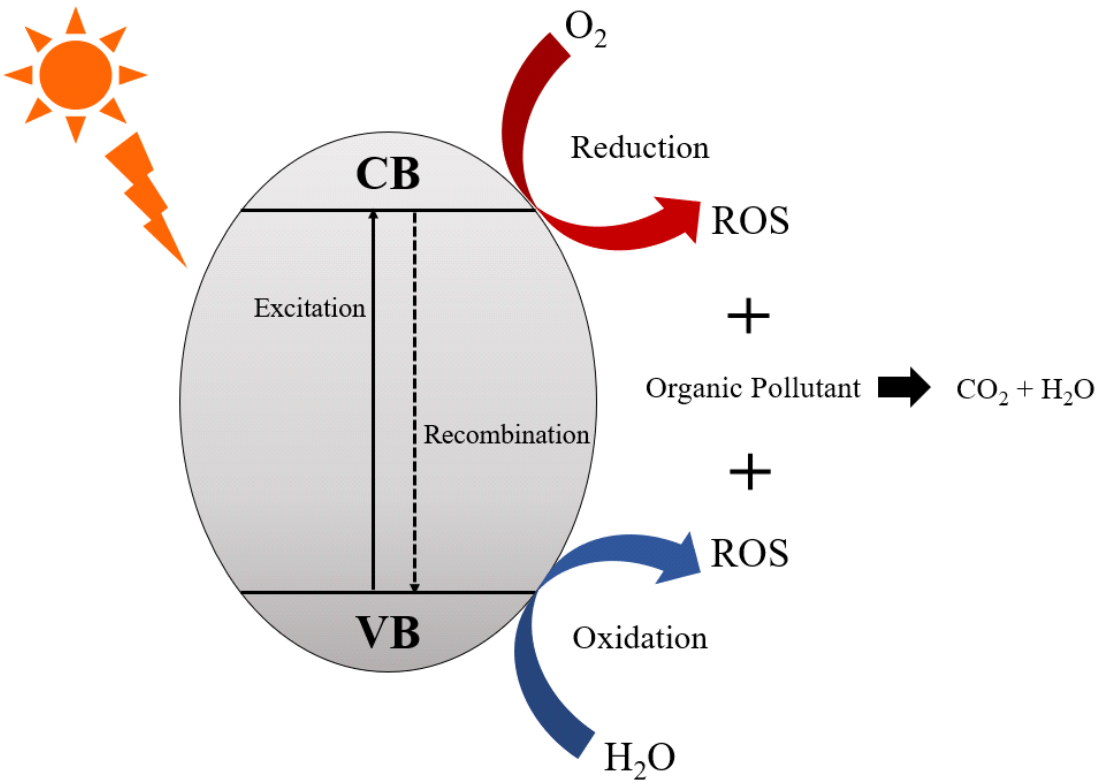

Figure. 2 Scheme of the operating of photocatalysts

2. AOPs

Advanced Oxidation Processes (AOPs) represent a sophisticated class of technologies in environmental engineering aimed at the mineralization and degradation of organic pollutants through the generation of Reactive Oxygen Species (ROS). Characterized by their high oxidation efficiency and speed in treating a wide range of organic contaminants, AOPs are considered the ideal solution for pollution control due to the non-toxic nature of their end products, chiefly CO_2 and H_2O. Among the myriad of methods employed, ozone-based [16], photocatalytic [17], Fenton and Fenton-like processes [18], electrochemical reactions [19,20], and sonolysis [21,22] are notable.

Photocatalytic AOPs, in particular, function under the influence of solar or UV light, activating a photocatalyst material (predominantly TiO_2) on whose surface ROS are generated. These ROS, including hydroxyl radical ($^{\bullet}OH$), hydrogen peroxide (H_2O_2), superoxide anion radical ($O_2^{\bullet-}$), and nitric oxide (NO), exist in various forms, each with a distinct reduction potential that influences their reactivity with organic pollutants. The hydroxyl radical, with its high reduction potential ($E^{\circ} = +2.80$ V vs. NHE) [23], is capable of reacting with almost all organic compounds, rendering it the most critical ROS in the context of AOPs. The table below summarizes the key ROS utilized in photocatalytic AOPs along with their reduction potentials [24].

ROS	Molecular Formula	Reduction Potential
Hydroxyl radical	$^{\bullet}OH$	2.80 eV
Ozone	O_3	2.07 eV
Hydrogen peroxide	H_2O_2	1.78 eV
Singlet oxygen	$^1O_2$	1.52 eV
Nitric oxide	NO	0.96 eV

The effective generation and utilization of ROS are pivotal in maximizing the performance of photocatalytic AOPs. Through these mechanisms, photocatalytic AOPs contribute to the mineralization of recalcitrant organic pollutants, detoxification of heavy metals, thereby the protection of the environment and sustainable water management. This highlights the integral role of advanced oxidation in modern environmental remediation strategies, underscoring the necessity for ongoing research and development in this critical field.

3. Cu_xP

Copper phosphide (Cu_xP) has been recognized as a promising candidate material for various applications including batteries, photo/electro catalyst, and water splitting, owing to its unique physicochemical properties. Notably, this material is thermally stable, environmentally friendly, and cost-effective for mass production. Despite its extensive research across various domains such as hydrogen generation [25,26], environmental catalyst [27-29], water electrolysis [30], CO_2 reduction [31], and battery materials [32,33], studies on its utilization as an environmental catalyst remain relatively scarce.

In this context, photocatalytic water treatment research utilizing Cu_xP offers a new perspective. For instance, one study employed Cu_3P as a peroxydisulfate (PDS) activator for the degradation of organic matter, demonstrating the significant advantage of utilizing sulfate radicals, which are highly oxidative species generated through PDS activation [34], for the decomposition of organic pollutants [28]. However, this approach required the additional introduction of PDS, marking a drawback. Another study coated Hydroxyapatite (HAp) surfaces with Copper Phosphate to modulate HAp surface activity and activate PDS for water treatment [29]. This research highlighted the use of $Cu_3(PO_4)_2$ not for the direct decomposition of organic pollutants but as a means to regulate the activity on HAp surface, with the limitation of involving an additional chemical, PDS too.

This study is predicated on the ability of Cu_xP to spontaneously oxidize

oxygen to generate hydrogen peroxide in acidic aqueous solutions (pH 3), which then leads to the formation of hydroxyl radicals and subsequent decomposition of organic pollutants [35]. This process suggests the feasibility of decomposing aqueous pollutants without the need for any additional chemical supply. However, the decline activity in acidic solutions and the leaching of copper and phosphide were pointed out as significant limitations affecting the efficiency of pollutant degradation in water.

Therefore, this research aims to develop a photocatalytic water treatment system that maintains the ROS generation capability of Cu_xP while ensuring high stability under neutral or alkaline conditions. To handle the issue of reduced activity with increasing pH, visible light was utilized as an additional energy source. The system developed in this study exhibited unique properties of controlling ROS under specific conditions by adjusting the presence of visible light and pH, achieved without the input of additional chemicals such as PDS or PMS (peroxymonosulfate). The structure and surface characteristics of Cu_xP were studied using various analytical instruments, and the mechanism of $^{\bullet}OH$ and $^1O_2$ generation and the decomposition of aqueous organic pollutants were verified through the use of various scavenger and the probe under different reaction conditions.

Ⅱ. Experiment

1. Materials

The chemicals used in the experiment are listed below.

Ccopper hydroxide ($Cu(OH)_2$, Aldrich), sodium hypophosphite monohydrate ($NaH_2PO_2•H_2O$, Aldrich) was used to synthesis Cu_xP. And furfuryl alcohol (FFA, Aldrich), phenol (Junsei), 4-chlorophenol (Aldrich), benzoic acid (Sigma-Aldrich), ranitidine (Sigma-Aldrich), acetaminophen (Aldrich), carbamazepine (Aldrich), cimetidine (Sigma), phosphate buffered saline solution (PBS, Sigma-Aldrich), tert-butanol (t-BuOH, Aldrich), L-histidine (Sigma-Aldrich), deuterium oxide (D_2O, Sigma-Aldrich), coumarin (Sigma), N,N-diethyl-1,4-phenylene-diamine sulfate (DPD, Sigma-Aldrich), superoxide dismutase from bovine erythrocytes (SOD, Sigma), humic acid (HA, Suwannee River), fulvic acid (FA, Suwannee River), sodium chloride (NaCl, Sigma-Aldrich), sodium nitrate ($NaNO_3$, Sigma-Aldrich), sodium bicarbonate ($NaHCO_3$, Sigma-Aldrich), 5,5-dimethyl-1-pyrro-line-N-oxide (DMPO, Sigma-Aldrich), and 2,2,6,6,-tetramethyl-4-piperidone (TEMP, Aldrich) were used for Cu_xP experiments and mechanism analysis.

All chemicals are ready to use without further purification, and experiments were performed using ultrapure deionized water as the aqueous solution.

2. Synthesis of Copper Phosphide

Cu_xP was synthesized according to the synthetic method reported in previous studies. Firstly, 0.1 g of $Cu(OH)_2$ and 0.6 g of $NaH_2PO_2•H_2O$ were accurately weighed and mixed homogeneously. The mixture was placed in a crucible boat for calcination. The calcination process was conducted in a tube furnace at 300 °C for 2 hours, with a ramping rate of 2 °C/min, under an Ar atmosphere. The resulting Cu_xP was subsequently ground, dispersed in 200 mL of distilled water, and sonicated in an ultrasonic bath for 1.5 hours. Following sonication, the dispersion was filtered through a membrane filter with a 0.45 μm pore size and rinsed multiple times with distilled water. The filtered sample was then dried in an oven at 80 °C, yielding the Cu_xP as a black powder.

3. Characterization Methods

The physicochemical properties of the Cu_xP were analyzed using a diverse array of instruments. Crystal structure was examined with X-ray Diffraction (XRD, D8 Focus, Bruker), Fourier-transform Infrared Spectroscopy (FT-IR, NICOLET iS10, Thermo Scientific), and Raman Spectroscopy (In Via Raman Microscope, Renishaw). Surface characteristics were determined via X-ray Photoelectron Spectroscopy (XPS, K-Alpha+, Thermo Scientific). UV-visible Absorption Spectroscopy (UV-2401PC, Shimadzu) was utilized for assessing absorption properties. For particle size and structure analysis, Field-Emission Scanning Electron Microscopy and Energy-Dispersive X-ray Spectroscopy (FE-SEM and EDS, Inspect F50, CIQTEK) alongside High-Resolution Transmission Electron Microscopy (HR-TEM, Titan 80-300™ microscope, Thermo Scientific) were employed.

4. Activity of Cu_xP

Experiments were conducted in a 50 mL Pyrex reactor, with all tests carried out using a volume of 30 mL. The amount of Cu_xP was determined experimentally to be optimal at 1 g/L, as illustrated in Fig. 3 Initial pH were adjusted using perchloric acid ($HClO_4$) or sodium hydroxide (NaOH). The concentration of the organic pollutants was appropriately selected within the range of 20 to 100 μM. Under dark conditions, Cu_xP was dispersed in distilled water using an ultrasonic bath, followed by pH adjustment before initiating the reaction with the addition of the pollutant. Under visible light conditions, Cu_xP and the pollutant were introduced, followed by pH adjustment and dispersion using ultrasonic bath. Prior to light irradiation, the mixture was allowed to air-equilibrate for 30 minutes in the dark. The reaction was initiated with visible light irradiation, employing a Xe arc lamp (300W, Oriel) as the light source. A cut-off filter was utilized to ensure visible light ($\lambda > 420$ nm) irradiated, and the aqueous solution was continuously stirred throughout all experimental processes.

From the start to the end of the reaction, 1 mL samples of the suspension were extracted at regular intervals using a syringe and then filtered through a syringe filter to remove the Cu_xP. For the assessment of stability, repetitive experiments were conducted under dark/pH 3 and visible light/pH 7 conditions. The concentration of FFA was fixed at 100 μM for dark/pH 3 and 20 μM under visible light/pH 7. After each cycle, Cu_xP was recovered by filtration through a membrane filter with a pore

size of 45 μm and then dispersed in a new suspension for reuse. The repetition frequency was set at 10 cycles for dark/pH 3 conditions and 5 cycles for visible light/pH 7 conditions.

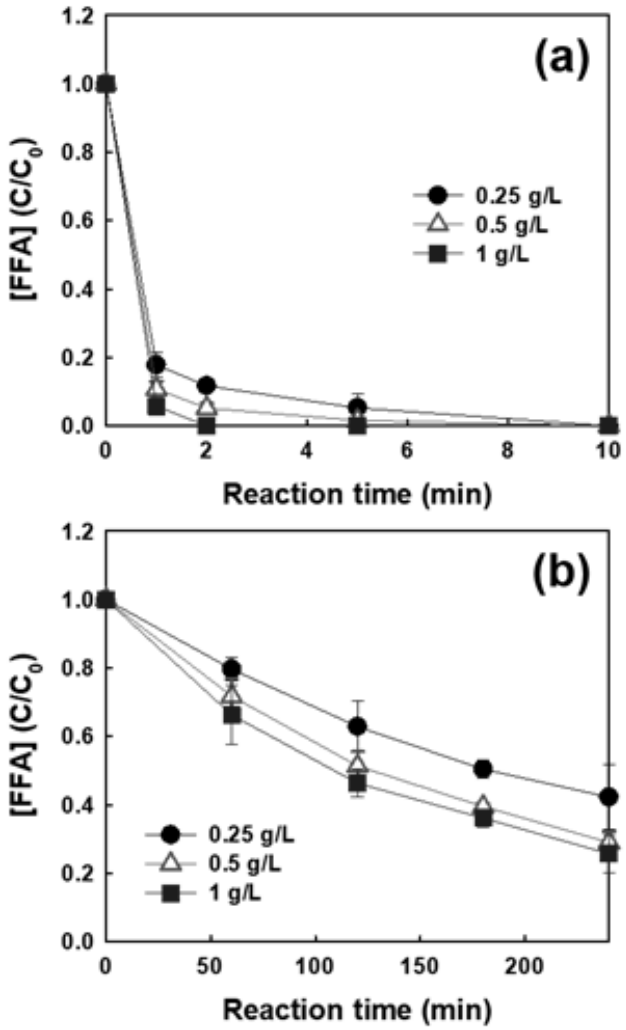

Figure. 3 Impact of Cu_xP Concentration on the FFA degradation (a) at dark/ pH 3 and (b) under visible light irradiation(λ > 420 nm)/ pH 7 ($[FFA]_0$ = 20 μM)

5. Analysis

The concentrations of organic pollutants, including Phenol, 4-Chlorophenol, Benzoic Acid, Ranitidine, Acetaminophen, Carbamazepine, and Cimetidine, were quantitatively analyzed using High-Performance Liquid Chromatography (HPLC Agilent 1220 Infinity II). The system was equipped with a variable wavelength detector and a ZORBAX 300SB-C18 column for precise separation and detection.

The concentration of hydrogen peroxide was determined using a UV/visible spectrophotometer (Analytik Jena Specord 210 Plus) employing the colorimetric method with N,N-diethyl-p-phenylenediamine (DPD) as the analytical reagent.

The generation of hydroxyl radicals ($^{\bullet}OH$) was measured through a fluorescence method using a spectrofluorometer (HORIBA, Fluoromax 4CTCSPC). In this analysis, coumarin served as the $^{\bullet}OH$ trapping agent. The oxidation of coumarin by $^{\bullet}OH$ yields 7-hydroxycoumarin (7-HC), allowing the assessment of $^{\bullet}OH$ production by measuring the concentration of 7-HC. The fluorescence of 7-HC was detected at 460 nm with excitation at 332 nm.

The presence of humic and fulvic acids was determined by monitoring their fluorescence emission utilizing a spectrofluorometer (HORIBA fluoromax-4).

The amounts of dissolved Cu and P species from the Cu_xP suspension were evaluated using Inductively Coupled Plasma Optical Emission Spectroscopy (ICP-OES-6300, Thermo Scientific).

6. Mechanism and EPR analysis

To investigate the effect of oxygen on the decomposition of FFA, experiments were conducted by pugging oxygen and argon into the reactor, creating environments that were oxygen-rich or devoid of oxygen. To understand the impact of $^{\bullet}OH$, $^{1}O_2$, and $O_2^{\bullet-}$, scavengers such as tert-butanol (t-BuOH), L-histidine, and SOD were introduced, allowing for the analysis of the ROS predominantly involved in the reaction, thereby elucidating the reaction mechanism. Additionally, in the scavenger tests using L-histidine, experiments were performed using D_2O instead of distilled water to extend the short lifetime of $^{1}O_2$, thus clarifying the analysis of the reaction mechanism.

Electron Paramagnetic Resonance (EPR) analysis utilized to detect the presence of singlet oxygen ($^{1}O_2$) and hydroxyl radical ($^{\bullet}OH$) using the spin-trapping agents as 2,2,6,6-tetramethyl-4-piperidone (TEMP) for $^{1}O_2$ and 5,5-dimethyl-1-pyrroline-N-oxide (DMPO) for $^{\bullet}OH$, respectively. EPR signals of the TEMP-$^{1}O_2$ and DMPO-$^{\bullet}OH$ spin adducts were monitored using an EPR spectrometer (JES-X310, JEOL). The measurement conditions were as follows: fat cell 0.2 mL, microwave power 10 mW, microwave frequency 9.42 GHz, center feld 337 mT, and modulation width 0.1 mT.

Ⅲ. Results and Discussion

1. Characterization of Copper Phosphide

X-ray diffraction patterns (Fig. 4a) indicates that the Cu_xP compound predominantly consists of hexagonal phase Cu_3P and monoclinic phase CuP_2, with Cu_3P exhibiting notably higher diffraction peak intensities compared to CuP_2 [36,37]. This suggests a preferential formation of larger Cu_3P crystals during synthesis. Additionally, Raman spectroscopic investigation revealed a distinct peak at 420 cm^{-1} (Fig. 4b), indicative of the Cu_3P phase, further corroborated by the characteristic spectrum of copper phosphide surrounded by an amorphous carbon layer [38].

To investigate the surface oxidation characteristics of Cu_xP, we performed an in-depth analysis using high-resolution XPS. The analysis detected distinct peaks in Fig. 4c,d corresponding to copper, phosphorus, and oxygen elements without any trace of impurities. Specifically, peaks at 933.0 and 952.9 eV were identified as belonging to the Cu^+ $2p_{3/2}$ and Cu^+ $2p_{1/2}$ states in Cu_3P. In contrast, peaks at 935.1 and 955.1 eV were associated with the Cu^{2+} $2p_{3/2}$ and Cu^{2+} $2p_{1/2}$ states in CuP_2 [38,39]. As depicted in Figure 1d, the P 2p spectrum analysis revealed three distinct peaks, with those centered at 129.1 and 130.1 eV linked to P-P bonding in both Cu_3P and CuP_2, and a broad peak at 133.3 eV indicative of oxidized phosphorus. The relative peak intensities of P-O to P-P bonds suggest that oxidized phosphorus predominates on the Cu_xP surface.

The study further delved into the morphological and elemental

composition of Cu_xP through field emission scanning electron microscopy (FE-SEM), high-resolution transmission electron microscopy (HR-TEM), and energy-dispersive X-ray spectroscopy (EDS). FE-SEM image (Fig. 4f) showcased sheet-covered structures with visible particle aggregation certain regions. HR-TEM image (Fig. 4g) revealed an amorphous layer on the Cu_xP surface, signifying a homogeneous distribution of oxidized phosphorus, which was confirmed through EDS mapping (Fig. 4h,i) that showed a consistent dispersion of copper, phosphorus, and oxygen, devoid of any impurities. (refer to Figures 1h and 1g). Thus, when only Cu_3P and CuP_2 are present, Cu_xP comprises 93.2% Cu_3P and 6.8% CuP_2.

Analysis via UV-visible diffuse reflectance spectroscopy (UVDRS) revealed that the bandgap of Cu_xP measures at 1.71 eV, as shown in Fig. 4e The equation for calculating the valence band potential (E_{VB}) is given as Eq. (6).

$$E_{VB} = X - E_e + 0.5\ E_g. \quad (6)$$

With X denoting the absolute electronegativity of Cu_3P at 4.69 eV, E_e representing the free electron energy on the hydrogen scale at 4.5 eV, and E_g the bandgap at 1.71 eV, the E_{VB} is thus calculated to be 1.045 eV [40].

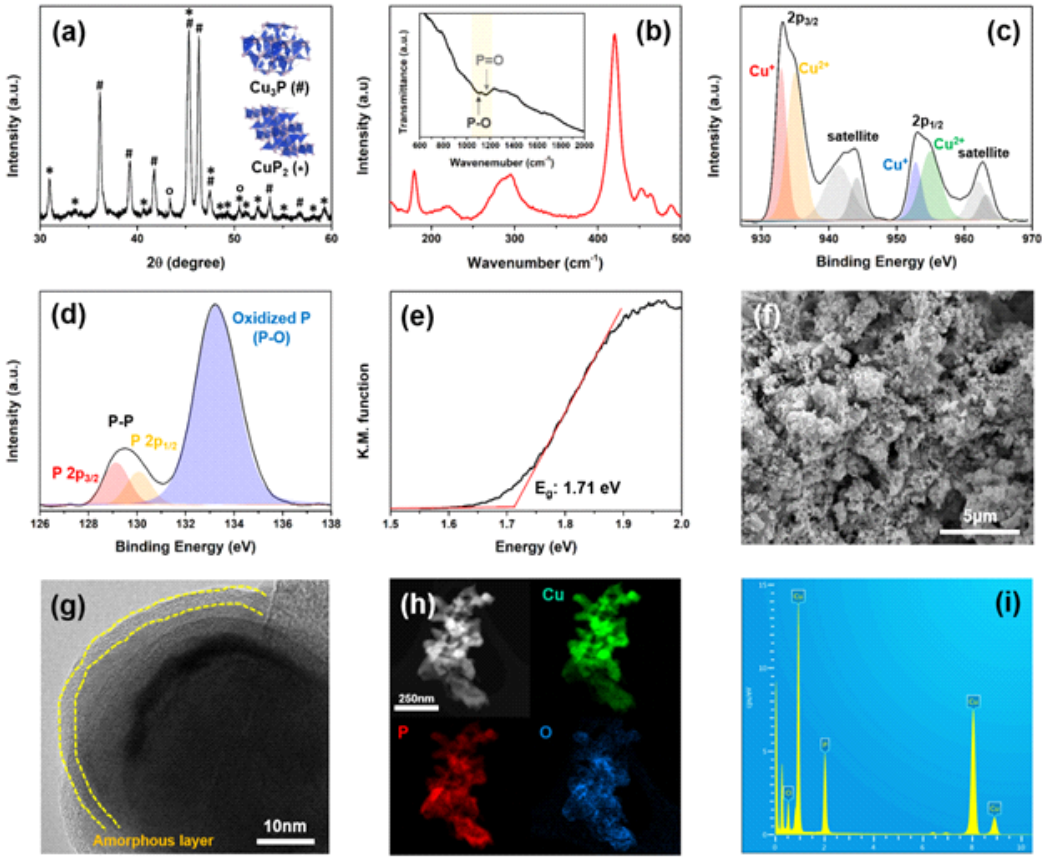

Figure. 4 (a) XRD pattern denoted as CuP_3(#) and CuP_2(∗), (b) Raman spectrum (the inset shows the FT-IR spectrum), XPS spectra of (c) Cu 2p and (d) P 2p, (e) UVDRS spectrum, (f) FE-SEM and (g) HR-TEM images, (h) EDS elemental mapping, and (i) the spot profile EDS spectrum of Cu_xP.

2. Activity of Cu_xP

To assess the influence of pH and light on the Cu_xP, time-dependent experiments focused on the decomposition of Furfuryl Alcohol (FFA) were carried out. FFA is recognized as an efficient $^1O_2$ probe molecule due to its rapid reaction rate with $^1O_2$ ($k = 1.2 \times 10^8\ M^{-1}\ s^{-1}$), making it an exemplary subject for exploring the formation and role of $^1O_2$ in reactions [41,42]. The experimental setup aimed to elucidate the effects of 'the presence of light' and 'pH' on the reaction by performing decomposition experiments under both dark conditions and visible light irradiation ($\lambda > 420$ nm), with initial pH values set to 3, 5, 7, 9, and 11. Aside from the light conditions and initial pH, all other experimental parameters were maintained constant. The decomposition efficiency of FFA under both dark and visible light irradiation across varying pH levels is depicted in Fig. 5 in conditions of both dark and visible light irradiation, the reaction at an initial pH 3 completed within 2 minutes, showcasing a rapid decomposition of FFA. At pH 5, the decomposition process decelerated, concluding within 10 minutes, which aligns with findings from previous study. This indicates that the acidity of the solution, rather than the exposure to light, predominantly influences the behavior of Cu_xP, particularly in acidic aqueous solutions where the pH is low.

A notable observation in neutral and alkaline aqueous solutions, specifically at above pH 7, was the difference in FFA decomposition efficiency under dark and visible light irradiation. In dark, at neutral pH

7 and in alkaline solutions at pH 9 and 11, no reaction was observed over a 2-hour experiment period, and the concentration of FFA remained consistent, as reported (Fig. 5a). However, under visible light irradiation, significant reductions in FFA concentration were observed over time in solutions at pH 7 and 9, while almost no reaction was apparent in strongly alkaline conditions at pH 11 (Fig. 5b). This fascinating result, where FFA degradation that was unfeasible under dark at neutral or alkaline pH levels becomes possible under visible light irradiation, suggests that the catalytic behavior of Cu_xP in solutions with neutral or higher pH values is transformed by the introduction of visible light acting as an additional energy source.

This is a pioneering discovery, indicating the potential application of Cu_xP as photocatalysts and the unveiling of novel photocatalytic mechanisms activated by visible light. Synthesizing these outcomes, the effects of pH and light on Cu_xP reactions were thoroughly analyzed, establishing dark/pH 3 and visible light/pH 7 as representative conditions for further investigation.

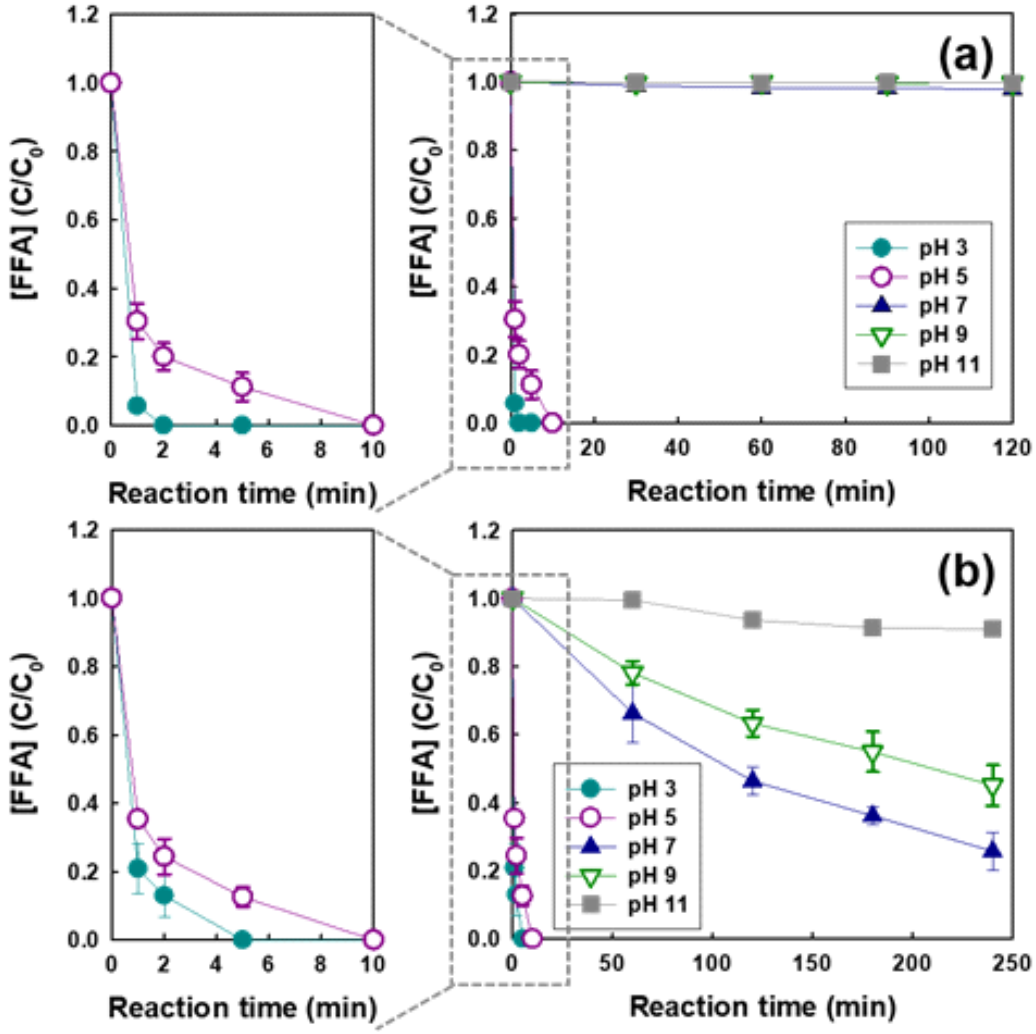

Figure. 5 Decomposition efficiency of FFA according to initial pH under (a) dark and (b) visible light (λ > 420 nm) irradiation ($[Cu_xP]_0$ = 1 g/L, $[FFA]_0$ = 20 μM).

3. Mechanism analysis

1) pH 3/dark: hydroxyl radical

To elucidate the precise reaction mechanisms and to identify the dominant ROS involved in the reaction under the dark/pH 3, an extensive analysis was conducted using a variety of ROS scavengers and probes. The experiments revealed that, in dark at pH 3, Cu_xP spontaneously reducted oxygen to produce hydrogen peroxide, which is subsequently generate hydroxyl radicals, leading to the decomposition of organic compound through a series of consecutive reactions (Eq (7),(8)).

$$O_2 + 2H + 2e^- \rightarrow H_2O_2 \quad (7)$$

$$H_2O_2 + e^- \rightarrow {}^{\bullet}OH + OH^- \quad (8)$$

Under the same conditions as previous experiments, the decomposition of FFA was performed to investigate the role of oxygen and the impact of $^{\bullet}OH$. For this purpose, argon (Ar) purging and t-BuOH were utilized respectively, where Ar serves to create an anoxic condition by displacing oxygen, and t-BuOH acts as a representative $^{\bullet}OH$ scavenger.

The experimental outcomes, in the presence of Ar (without O_2) and t-BuOH, exhibited distinct trends from previous observations. The concentration of FFA remained constant and unchanged as shown in Fig. 6a, indicating ⅰ) Oxygen serves as the initiator of the reaction, and ⅱ) the decomposition of FFA is facilitated by $^{\bullet}OH$. Fig. 6d provides a

clearer illustration of these findings by depicting the FFA removal efficiency. This inference is supported by the data in Fig. 6b, which shows the highest production of hydrogen peroxide under oxygen-rich conditions, suggesting the involvement of oxygen in the Cu_xP reaction. Furthermore, under atmospheric conditions, the production of hydrogen peroxide decreased to half, and similar to the decomposition of FFA, ceased entirely upon Ar purging. The observation that hydrogen peroxide production does not increase but rather reaches equilibrium five minutes after the experiment begins can be explained by the real-time reduction of hydrogen peroxide generated from oxygen into $^{\bullet}OH$ [43].

The generation of $^{\bullet}OH$ from hydrogen peroxide was unequivocally confirmed through the formation of 7-hydroxyl coumarin (7-HC) using coumarin, a $^{\bullet}OH$ detector that rapidly reacts with $^{\bullet}OH$ to produce 7-HC (Eq. (9)).

$$\text{coumarin} + {}^{\bullet}OH \rightarrow \text{7-hydroxyl coumarin (7-HC)} \quad (9)$$

The emission intensity at 460 nm, the emission wavelength of 7-HC, is depicted in Fig. 6c As anticipated, the formation of $^{\bullet}OH$ increased over time. In contrast, in the presence of Ar, the sequential reactions starting from oxygen were interrupted, resulting in no formation of 7-HC.

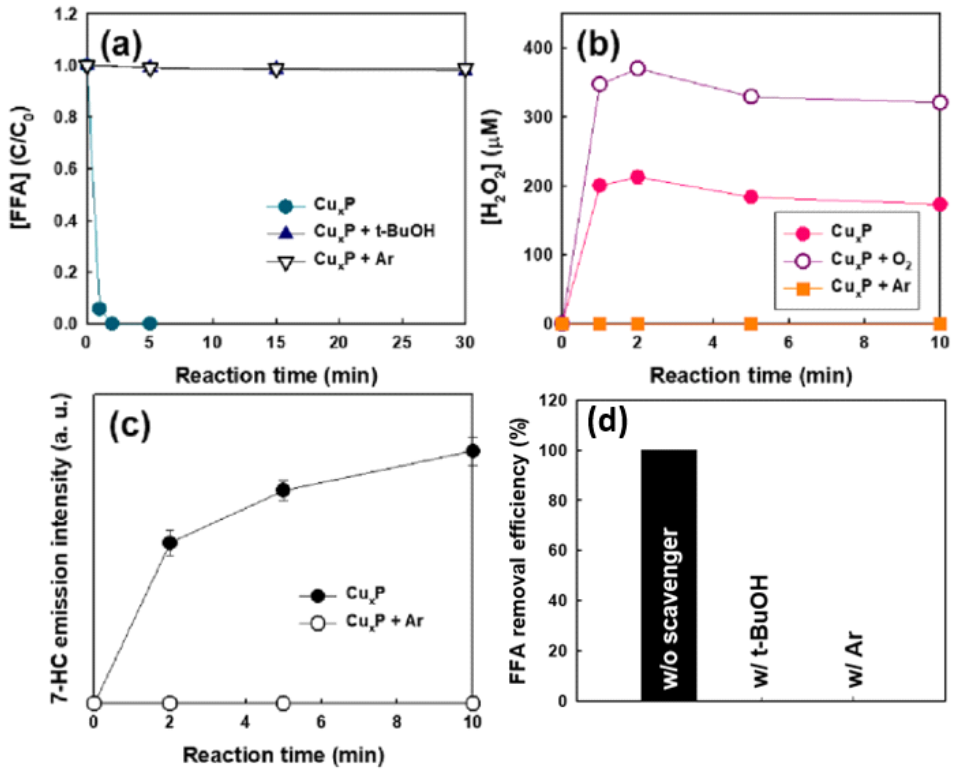

Figure. 6 (a) Effects of t-BuOH and Ar-saturated (anaerobic environment) on FFA degradation, (b) Effects of O_2-saturated and Ar-saturated conditions on generating H_2O_2, (c) The generation of 7-HC under Ar purging at pH 3 dark condition and (d) Efficiency of FFA removal with t-BuOH and under Ar purging at a pH 3 in dark conditions.

3. Mechanism analysis

2) pH 7/visible light: singlet oxygen

In neutral aqueous solutions under visible light irradiation, Experiments were conducted using ROS scavengers and probes to identify the primary oxidizing agent involved. In the presence of L-histidine ($^1O_2$ scavenger), the catalytic reaction did not occur. Substituting distilled water with deuterium oxide (D_2O) accelerated the reaction compared to initial results (Fig 7a). These support the assertion that under visible light irradiation at pH 7, singlet oxygen acts as the dominant oxidant in the decomposition of FFA facilitated by Cu_xP catalysts. In water-based systems, the duration of $^1O_2$ presence ranges between microseconds to milliseconds. However, an increased lifespan of $^1O_2$ is noted in the presence of D_2O a phenomenon attributable to the H-D isotopic effect. [44,45]. This effect, which involves the transfer of energy from electronic to vibrational states, significantly stabilizes and extends the life of $^1O_2$. As a result, the rate of non-radical reactions within D_2O is substantially accelerated. Under Ar-purging (anaerobic environment) condition the decomposition of FFA was not observed. Such results emphasize the oxygen plays vital role in the generation of $^1O_2$.

Cu_xP, possessing a bandgap of 1.71 eV, absorbs energy upon exposure to exceeding its bandgap, leading to electron excitation and the subsequent formation of electron-hole pairs. During the recombination process of these electron-hole pairs, the released energy is transferred, resulting in

the formation of an excited singlet state of Cu_xP. Energy transfer then leads to the formation of an excited triplet state of Cu_xP through intersystem crossing. This excited triplet state is subsequently quenched by O_2, generating $^1O_2$.

Fig. 7b unequivocally demonstrate that the generation of $^1O_2$ is facilitated via an energy transfer mechanism. A pivotal experiment within this study involved the addition of Superoxide Dismutase (SOD), conclusively proving that the generation of $^1O_2$ is independent of any electron transfer mechanisms. The process of ROS generation through the electron transfer pathway mediated by superoxide ($O_2^{\bullet-}$) is as follows [46].

$$2O_2^{\bullet-} + 2H+ \rightarrow H_2O_2 + O_2 \text{ (SOD acts as a catalyst)} \quad (10)$$

$$H_2O_2 \rightarrow {}^{\bullet}OH + OH^- \quad (11)$$

However, despite the addition of SOD, which serves as both a catalyst for electron transfer reactions and a scavenger of $O_2^{\bullet-}$, the experimental outcomes remained unchanged. This unequivocally indicates that ROS generated through electron transfer do not contribute to this reaction mechanism. Theoretically, the addition of SOD should have accelerated the disproportionation of $O_2^{\bullet-}$, thereby reducing the generation of $^1O_2$. Contrary to this hypothesis, no alteration in the experimental results was observed, reinforcing that the generation of $^1O_2$ is not dependent by elecrton transfer pathway.

In conclusion, the generation of $^1O_2$ from Cu_xP is achieved not through

electron transfer, but via an energy transfer mechanism. Understanding this mechanism lays a crucial foundation for the efficient development of photocatalytic systems and contributes significantly to the field of material science and optoelectronic technology, providing insights into the control and manipulation of ROS.

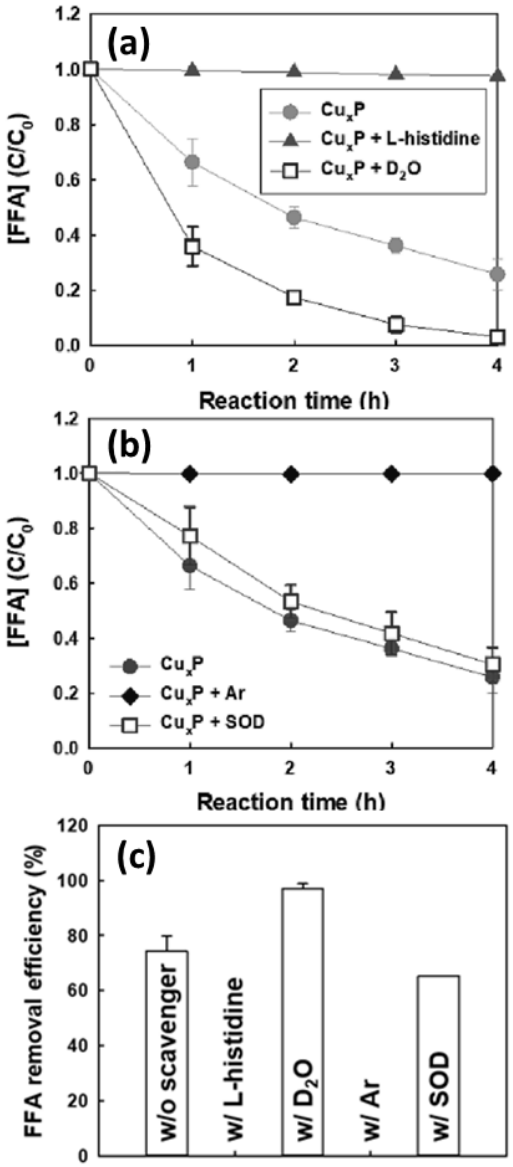

Figure. 7 Effect of (a) L-histidine, D_2O, (b) Ar-purging, SOD on FFA degradation in the suspension of Cu_xP at pH 7 under visible light (λ > 420 nm) and (c) FFA removal efficiency within the presence of L-histidine, D_2O, Ar-saturated and SOD conditions at pH 7 under visible light.

3. Mechanism analysis

3) EPR analysis

In this water-treatment-system utilizing Cu_xP, under dark at pH 3, hydroxyl radical ($^{\bullet}OH$) generated from H_2O_2 through electron transfer are observed, while under visible light irradiation at pH 7, singlet oxygen ($^1O_2$) is produced through energy transfer processes (Fig. 8). To substantiate this claim, EPR analysis was conducted. Since both $^{\bullet}OH$ and $^1O_2$ have short half-lives and disappear rapidly, their detection is challenging. Therefore, spin-trapping reagents that react with radicals to form stable adducts, making their detection possible in EPR, are used. DMPO for $^{\bullet}OH$ and TEMP for $^1O_2$ were used as spin-trapping agents. Under acidic conditions, $^{\bullet}OH$ peaks appeared 5 minutes after the reaction started, both with and without light (Fig. 9a). It is analyzed that H_2O_2 spontaneously generated from oxygen through Cu_xP in the initial 5 minutes, and the accumulated H_2O_2 is reduced through electron transfer. Therefore, the absence of $^{\bullet}OH$ peaks at 0 minutes is explained. At pH 7, peaks were only observed 5 minutes after the reaction commenced under visible light irradiation. This distinct in shape from the $^{\bullet}OH$ peak, indicates the generation of $^1O_2$ (Fig. 9b). For the production of $^1O_2$, firstly, an energy source, namely visible light irradiation, is required. Similar to the observation of hydrogen peroxide accumulation before the generation of $^{\bullet}OH$, $^1O_2$ is generated from initially formed triplet state of O_2 through energy transfer.

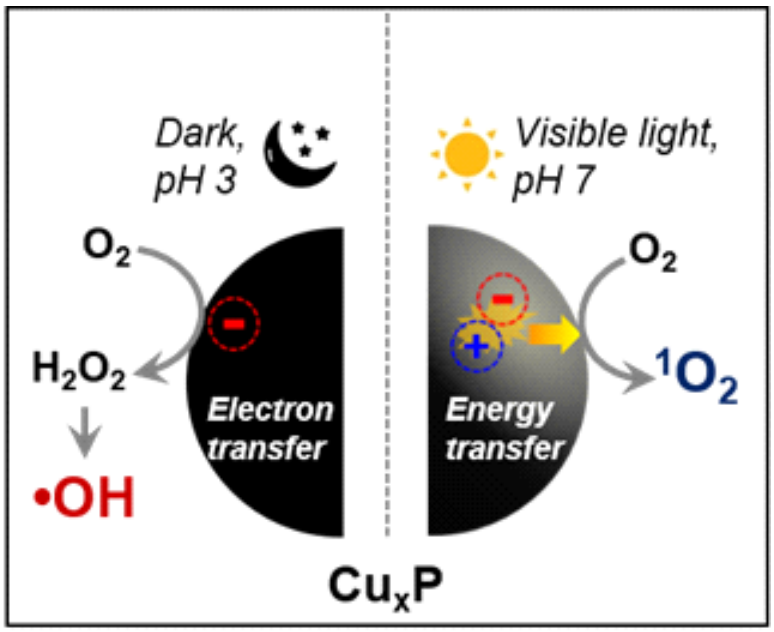

Figure. 8 Effect of (a) L-histidine, D_2O, (b) Ar-purging, SOD on FFA degradation in the suspension of Cu_xP at pH 7 under visible light (λ > 420 nm) and (c) FFA removal efficiency within the presence of L-histidine, D_2O, Ar-saturated and SOD conditions at pH 7 under visible light.

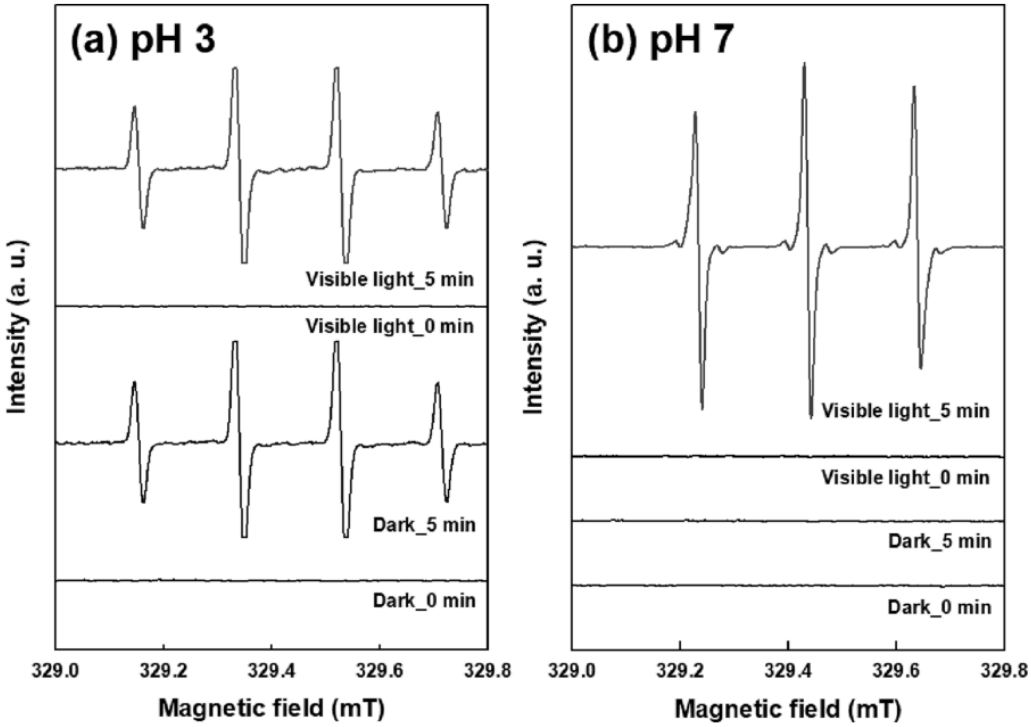

Figure. 9 EPR spectra of (a) $^{\bullet}$OH-DMPO adducts at pH 3 ($[DMPO]_0$ = 90 mM), and $^1O_2$-TEMP adducts at pH 7 ($[TEMP]_0$ = 0.17 M) formed in Cu_xP suspeneion under dark or visible light irradiation ($[Cu_xP]_0$ = 1 g/L and air-equilibrated).

4. Decomposition of organic compounds

In this section, we explored the degradation capabilities of Cu_xP towards phenolic compounds and pharmaceuticals. The treatment of such recalcitrant materials can be effectively addressed through AOPs.

Under dark conditions at a pH 3, a rapid and complete degradation of most organic pollutants was observed. The complete decomposition of Phenol, Cimetidine, and Carbamazepine occurred in less than 20 minutes, while the slowest degrading substances, Ranitidine and Benzoic acid, were substantially oxidized within 60 minutes (Fig. 10a). Under visible light irradiation at pH 7, a general trend of slower degradation for all organic substances compared to conditions at pH 3 was noted. Contrary to the dark at pH 3, significant variations in degradation rates were evident, attributed to the differential oxidation potentials of oxidative agents, indicating the non-selective oxidative potential of $^{\bullet}OH$ (2.80 eV) [23] and the selective oxidative potential of $^1O_2$ (1.52 eV) [24]. This supports the capability of Cu_xP to generate selective ROS. Under visible light irradiation at pH 7, Cimetidine and Acetaminophen were relatively quickly degraded, whereas the degradation of Benzoic acid and 4-Chlorophenol was slow (Fig. 10b). The notably slow degradation rate of Benzoic acid could be attributed to its slow reaction rate with $^1O_2$ ($k = \sim 10^6\ M^{-1}\ s^{-1}$) [47]. These differences arise from various factors such as the chemical structural stability of the pollutants, and interactions within the aquatic micro-environment, significantly impacting the efficiency of heterogeneous reactions in AOPs water treatments.

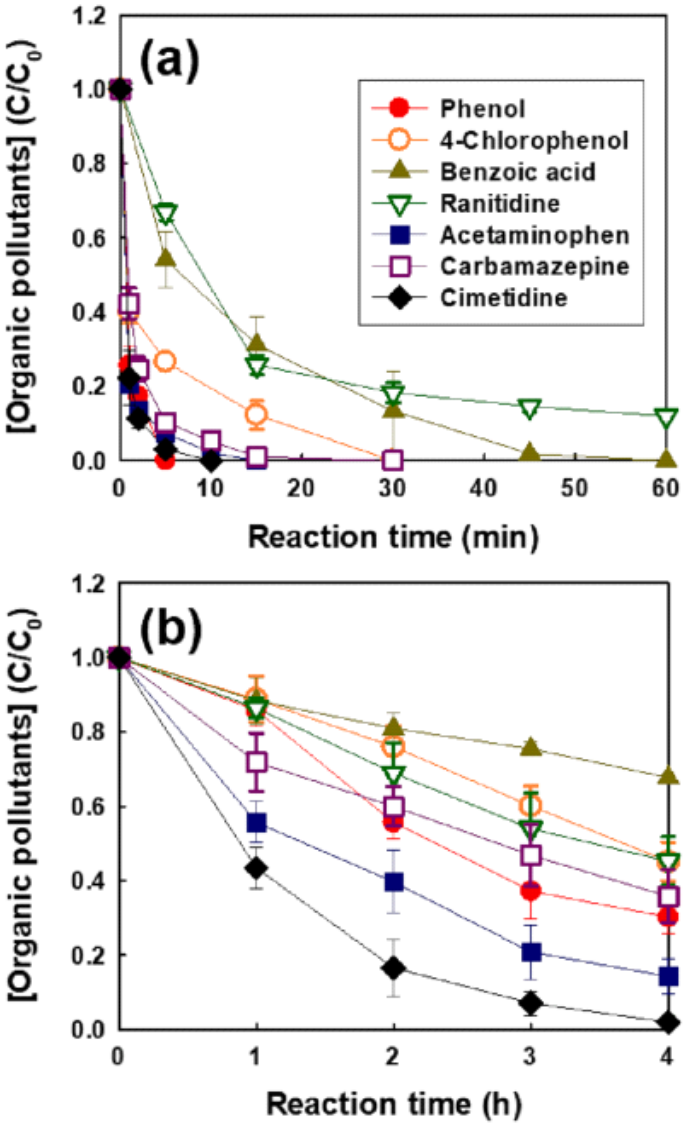

Figure. 10 Reduction of diverse organic pollutants through Cu_xP (a) at dark/ pH 3 and (b) under visible light irradiation (λ > 420 nm)/ pH 7 ($[Cu_xP]_0$ = 1 g/L, $[organic\ pollutants]_0$ = 20 μM).

In this experiment, we assessed the efficiency of FFA decomposition in the presence of Natural Organic Matters (NOMs) that represents organic substances in natural aquatic environments, various anions, and wastewater. It is generally known in water treatment research that NOMs or anions can decrease the efficiency of $^{\bullet}OH$-mediated AOPs. However, AOPs utilizing singlet oxygen ($^1O_2$) show minimal efficiency loss. Thus, $^1O_2$-mediated AOPs present a promising new AOPs technology for the removal of Pharmaceuticals and Personal Care Products (PPCPs), Endocrine Disrupting Chemicals (EDCs), and pesticides, addressing weaknesses associated with $^{\bullet}OH$-mediated AOPs reactions.

Our findings revealed a significant decrease in FFA decomposition efficiency under dark conditions at pH 3 in the presence of NOMs (SRHA, SRFA), indicating that the addition of chemical substances external to the reaction can lead to a drastic reduction in overall efficiency (Fig. 11a). This phenomenons was similarly observed in the presence of anions such as Cl^-, NO_3^-, and HCO_3^- (Fig. 11b). Conversely, under visible light irradiation at pH 7, the presence of NOMs and anions had negligible effects on the reaction (Fig. 11a,b).

The result of experiments using surface water and industrial wastewater as the background water showed in Fig. 11c. The presence of additional chemical substances in the aquatic environment under acidic conditions decreased the efficiency of FFA removal, with the most significant reduction observed in wastewater. Under neutral conditions with visible light irradiation, similar removal efficiencies were maintained across all water types. This consistency can be attributed to the minimal impact of

NOMs and ions on reactions involving $^1O_2$. This indicates the robustness of $^1O_2$-mediated AOPs under conditions that mimic real aquatic environments, highlighting the potential of Cu_xP as a versatile reagent for environmental remediation through AOPs.

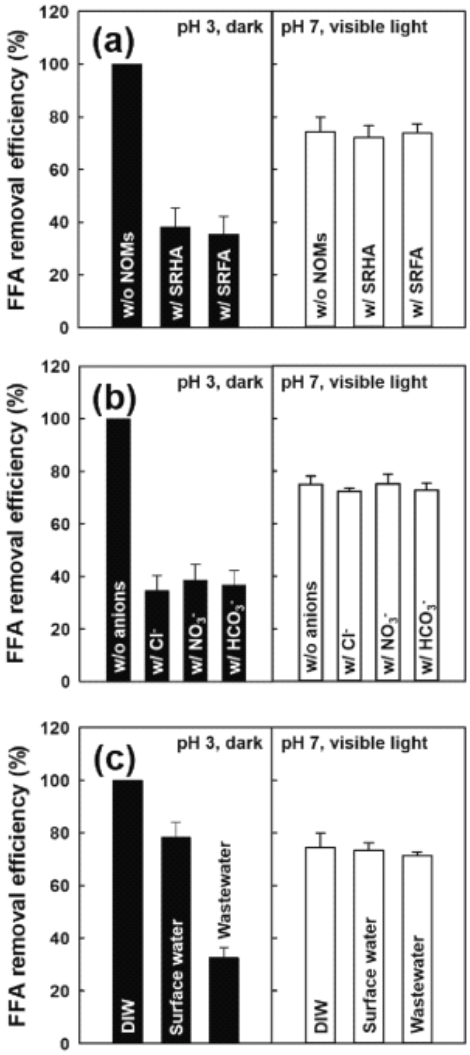

Figure. 11 Assessment of FFA decomposition capability in the presence of (a) NOMs, (b) anions, and (c) in actual surface water and wastewater. The dark bars (left) were obtained at pH 3 in the dark, and the white bars (right) were obtained at pH 7 under visible light irradiation ($[Cu_xP]_0$ = 1 g/L, $[FFA]_0$ = 20 μM, [NOMs] = 10 ppm and [anion] = 10 mM).

5. Inactivation of *E. coli*

The water treatment capability of Cu_xP through the generation of $^1O_2$ was also tested in bacterial inactivation experiments using Escherichia coli (*E. coli*) as a model organism. In a neutral environment under dark conditions, a slight decrease in the density of *E. coli* was observed. However, under illumination, the density of *E. coli* decreased rapidly, with complete inactivation achieved within 60 minutes. Interestingly, despite the presence of light, the addition of L-Histidine resulted in the scavenging of $^1O_2$, leading to no inactivation of *E. coli.* This highlights the critical role of $^1O_2$ in the bactericidal activity of the Cu_xP catalyst and underscores the importance of ROS generation conditions in the effective treatment of waterborne pathogens.

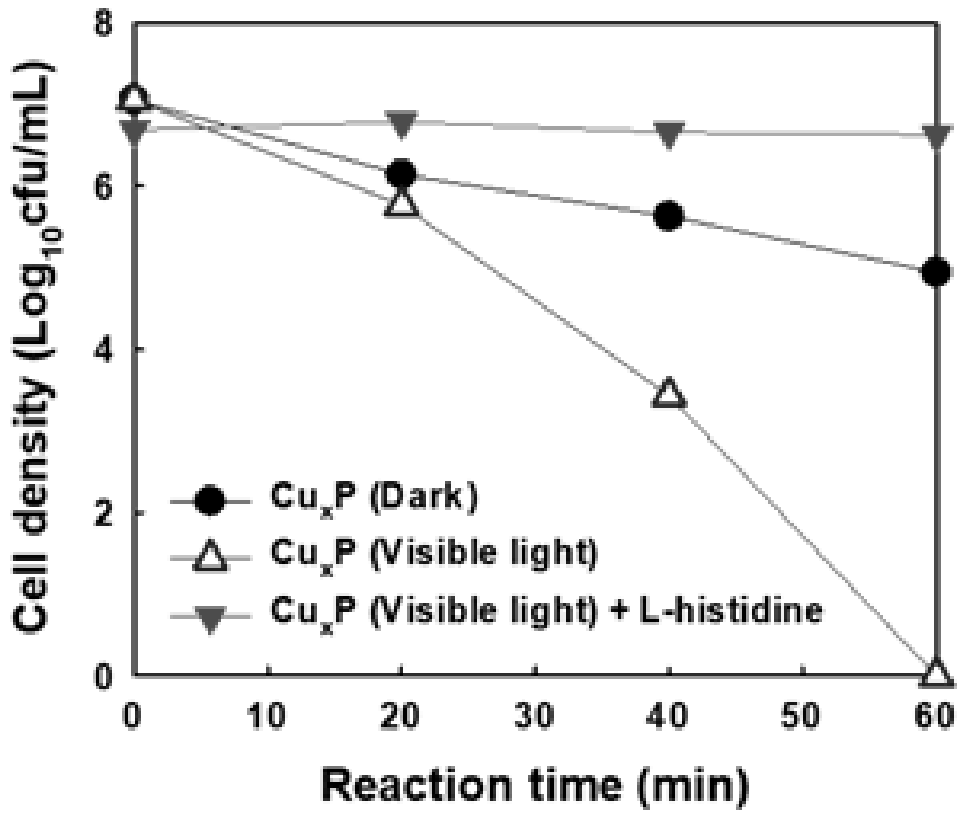

Figure. 12 *E. coli* inactivation dynamics in a Cu_xP suspension at pH 7, comparing dark with visible light exposure ($[Cu_xP]_0$ = 1 g/L and initial cell density = 107 cfu/mL).

6. Stability of Cu_xP

To assess the stability of the Cu_xP under different conditions (dark/pH 3, visible light/pH 7), repeated experiments for the decomposition of FFA were conceptualized. Previous studies have reported the phenomenon of leaching, where Cu and P ions from Cu_xP dissolve into the aqueous solution due to the 'acidic' nature (presence of hydrogen ions) of the solution.

Through repeated experimentation, we aimed to revalidate the Cu_xP compromised stability under acidic conditions and, notably, to verify improvements in catalyst stability within a neutral condition. For the repeated experiments, Cu_xP was recovered at the end of each cycle using a membrane filter, dispersed in a new solution, and reused. The results are presented in Fig. 13.

Under dark conditions at pH 3, consistent with previous findings, the stability of the Cu_xP gradually declined over 10 repeated experiments, with a rapid decrease in reactivity observed after exceeding five cycles. As shown in Fig. 13a, while the initial decomposition efficiency of FFA was very high, it gradually decreased, reaching around 30% by the 10^{th} repetition. The concentration of leached copper and phosphorus ions in the solution after 10 hours (after five cycles), as depicted in Fig. 13c, explains the significant deterioration in Cu_xP stability.

Contrarily, under visible light irradiation at pH 7, the outcomes were opposite. Despite repeated experiments, the stability did not decline, maintaining consistent FFA decomposition efficiency (Fig. 13b). As

evident from Fig. 13c, the leaching of Cu and P ions was negligible at pH 7. The high catalyst stability in neutral aqueous conditions was reaffirmed through Fig. 14c. After all repetitions were completed, the catalyst, upon recovery and analysis by XRD, exhibited peaks identical to those before experimentation, indicating that the repeated test did not affect the crystalline structure of Cu_xP. Comparative XPS results before and after the experiments also observed no changes (Fig. 14a,b).

Indeed, the varying stability of Cu_xP depending on the pH was visually evident throughout the experimental process. As shown in Fig. 15, with each additional cycle at pH 3, the solution color transitioned from black to progressively lighter gray due to Cu_xP leaching, whereas no color change in the solution was observed at pH 7.

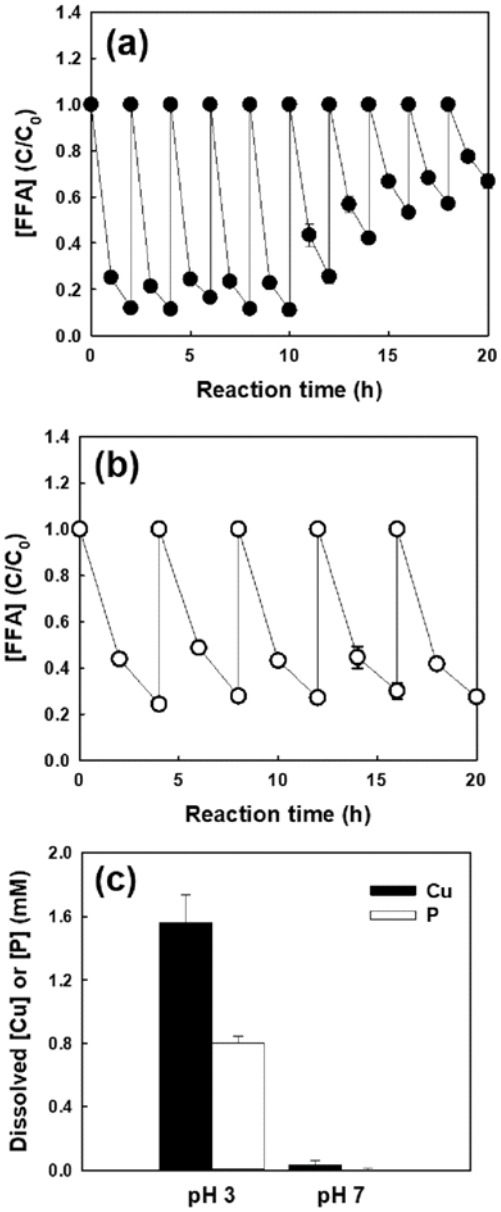

Figure. 13 FFA repeatedly decomposes FFA through Cu_xP at (a) pH 3/dark $[FFA]_0$ = 100 μM and (b) pH 7/visible light $[FFA]_0$ = 20 μM (c) Amounts of Cu and P species leached from Cu_xP after reacting for 4 hours.

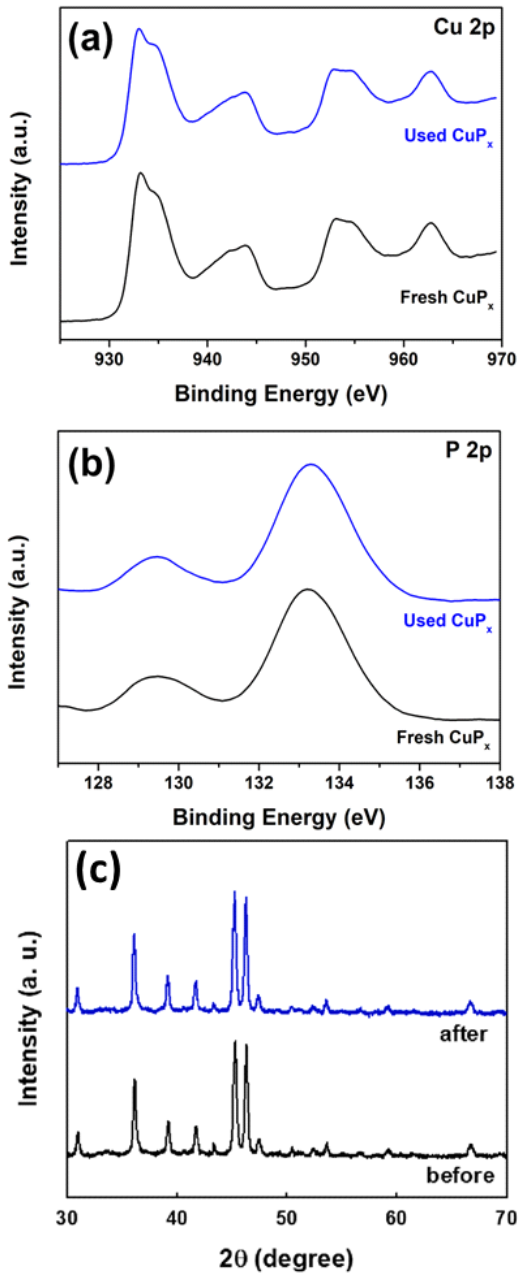

Figure. 14 Cu_xP XPS analysis for (a) Cu 2p and (b) P 2p used and fresh at pH 7 under visible light irradiation. (c) Comparison of Cu_xP XRD patterns, after and before repeated reaction at pH 7 under visible light.

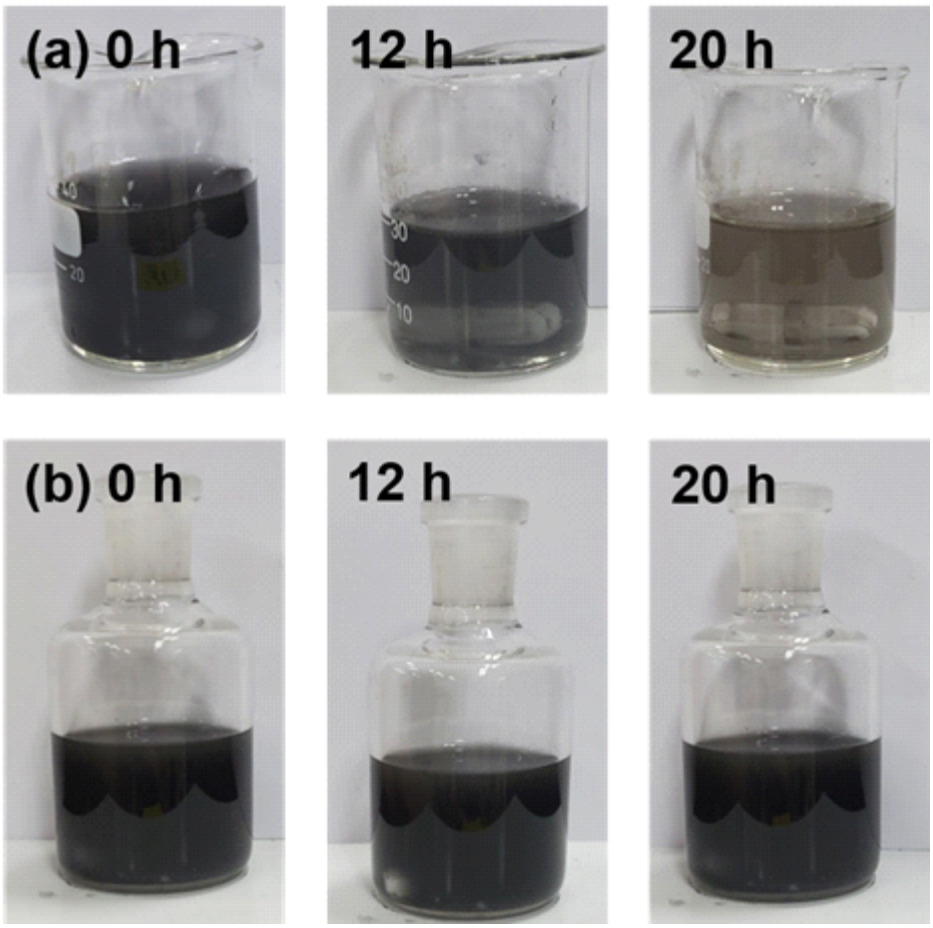

Figure. 15 The transformation in color of the Cu_xP suspension observed through multiple cycles of reaction, (a) in dark at pH 3 and (b) under visible light at pH 7.

Ⅳ. Conclusion

In the development of Cu_xP applicable to actual wastewater treatment processes, understanding the impact of diverse reaction conditions on targeted pollutants is imperative. This study demonstrated the selective production of ROS through Cu_xP by light on-and-off.

1) At pH 3 in the dark, Cu_xP acts as a solid reagent, spontaneously generating $^{\bullet}OH$ through a consecutive reactions by electron transfer (O_2 → H_2O_2 → $^{\bullet}OH$). $^{\bullet}OH$ is one of the most renowned ROS with a very high oxidation potential (2.80 eV), effectively oxidizing most organic materials non-selectively. Thus, $^{\bullet}OH$-based AOPs are suitable for treating recalcitrant organic pollutants.

2) Under visible light irradiation conditions at pH 7, a markedly different reaction mechanism was observed. The absorption of 420 nm visible light excites electrons, triggering energy transfer phenomena that lead to the production of $^1O_2$. $^1O_2$, being less susceptible to chemical reaction variability in aqueous environments compared to the radical attack-prone $^{\bullet}OH$-based AOPs is proposed as an alternative for PPCPs, EDCs, and pesticide treatment.

3) Such selective production of oxidants enhances the efficiency of AOPs-based wastewater treatments, enabling the appropriate selection of target pollutants based on the characteristics of each ROS. Furthermore,

the possibility of a continuous process through $^{\bullet}$OH-based AOPs following $^{1}O_2$-based wastewater treatment allows for the complete mineralization of recalcitrant substances.

4) Cu_xP exhibited gradual leaching and limited stability in acidic aqueous solutions. However, under neutral conditions with visible light irradiation, it demonstrated significant improvement in stability without any dissolution.

Reference

[1] Z. Shayegan, C.-S. Lee, F. Haghighat, TiO_2 photocatalyst for removal of volatile organic compounds in gas phase-a review, Chem. Eng. J. 334 (2018) 2408-2439.

[2] S. Fukahori, Y. Iguchi, H. Ichiura, T. Kitaoka, H. Tanaka, H. Wariishi, Effect of void structure of photocatalyst paper on VOC decomposition, Chemosphere 66 (2007) 2136-2141.

[3] H. Yu, K. Zhang, C. Rossi, Theoretical study on photocatalytic oxidation of VOCs using nano-TiO_2 photocatalyst, J. Photochem. Photobio. A Chem. 188 (2007) 65-73.

[4] S.-T. Lee, S.-J. Park, TiO_2 photocatalyst for water treatment applications, J. Ind. Eng. Chem. 19 (2013) 1761-1769.

[5] A. Houas, H. Lachheb, M. Ksibi, E. Elaloui, C. Guillard, J.-M. Herrmann, Photocatalytic degradation pathway of methylene blue in water, Appl. Catal. B Environ. 31 (2001) 145-157.

[6] D.S. Bhatkhande, V.G. Pangarkar, A.A.C.M. Beenackers, Photocatalytic degradation for environmental applications–a review, Chem. Technol. Biotechnol. 77 (2002) 102-116.

[7] K. Maeda, K. Teramura, D. Lu, T. Takata, N. Saito, Y. Inoue, K. Domen, Photocatalyst releasing hydrogen from water, Nature 440 (2006) 295.

[8] J. Hao, W. Yang, Z. Huang, C. Zhang, Superhydrophilic and superaerophobic
copper phosphide microsheets for efficient electrocatalytic hydrogen and oxygen evolution, Adv. Mater. Interfaces 3 (2016) 1600236.

[9] A. Kudo, Development of photocatalyst materials for water splitting, Int. J. Hydrogen Energy. 31 (2006) 197-202.

[10] X. Zhang, K.-A. Min, W. Zheng, J. Hwang, B. Han, L. Lee, Copper

phosphosulfides as a highly active and stable photocatalyst for hydrogen evolution reaction, Appl. Catal. B Environ. 273 (2020) 118927.
[11] J. Ran, M. Jaroniec, S.-Z. Qiao, Cocatalysts in semiconductor-based photocatalytic CO_2 reduction: achievements, challenges, and opportunities, Adv. Mater. 30 (2018) 1704649.
[12] J. Fu, K. Jiang, X. Qiu, J. Yu, M. Liu, Product selectivity of photocatalytic CO_2 reduction reactions, Mater. Today 32 (2020) 222-243.
[13] G. Sahara, I. Osamu, Efficient photocatalysts for CO_2 reduction, Inorg. Chem. 54 (2015) 5096-5104.
[14] P. Makuła, M. Pacia, W. Macyk, How to correctly determine the band gap energy of modified semiconductor photocatalysts based on UV-Vis spectra, J. Phys. Chem. Lett. 9 (2018) 6814-6817.
[15] 최원용, 이재상. "광촉매의 원리, 종류, 특성(성능) 및 개발현황" 공기청정기술 (2005) 1-8.
[16] J. Wang, Z. Bai, Fe-based catalysts for heterogeneous catalytic ozonation of emrging contaminants in water and wastewater, Chem. Eng. J. 312 (2017) 79–98.
[17] A. Shad, J. Chen, R. Qu, A.A. Dar, M. Bin-Jumah, A.A. Allam, Z. Wang, Degradation of sulfadimethoxine in phosphate buffer solution by UV alone, UV/PMS and UV/ H_2O_2: kinetics, degradation products, and reaction pathway, Chem. Eng. J. 398 (2020), 125357.
[18] G.-H. Moon, S. Kim, Y.-J. Cho, J. Lim, D.-H. Kim, W. Choi, Synergistic combination of bandgap-modified carbon nitride and WO_3 for visible light-induced oxidation of arsenite accelerated by in-situ Fenton reaction, Appl. Catal. B Environ. 218 (2017) 819-824.
[19] F. C. Moreira, R. A.R. Boaventura, E. Brillas, V. Vilar, Electrochemical advanced oxidation processes: a review on their application to synthetic and real wastewaters, Appl. Catal. B Environ. 202

(2017) 217-261.
[20] I. Sirés, E. Brillas, M. A. Oturan, M. A. Rodrigo, M. Panizza, Electrochemical advanced oxidation processes: today and tomorrow. a review, Environ. Sci. Pollut. Res. 21 (2014) 8336-8367.
[21] M. P. Rayaroth, U. K. Aravind, C. T. Aravindakumar, Ultrasound based AOP for emerging pollutants: from degradation to mechanism, Environ. Sci. Pollut. Res. 24 (2017) 6261-6269.
[22] M. P. Rayaroth, U. Aravind, C. T. Aravindakumar, Degradation of pharmaceuticals by ultrasound-based advanced oxidation process, Environ. Chem. Lett. 14 (2016) 259-290.
[23] M. Cheng, G. Zeng, D. Huang, C. Lai, P. Xu, C. Zhang, Y. Liu, Hydroxyl radicals based advanced oxidation processes (AOPs) for remediation of soils contaminated with organic compounds, Chem. Eng. J. 284 (2016) 582-598.
[24] H. R. Allcock, R. W. Allen, E. C. Bissell, L. A. Smeltz, M. Teeter, Phosphorus-nitrogen compounds 26 Molecular motion and molecular separations in cyclophosphazene clathrates, J. Am. Chem. Soc. 98 (1976) 5120-5125.
[25] H. Zhou, R. Chen, C. Han, P. Wang, Z. Tong, B. Tan, Y. Huang, Z. Liu, Copper phosphide decorated g-C_3N_4 catalysts for highly efficient photocatalytic H_2 evolution, J. Colloid Interface Sci. 610 (2022) 126-135.
[26] X. Li, J. Zhang, Y. Zhang, R. Zhang, D. Chen, C. Zhang, X. Zhang, B. Wang, H. Q. Luo*, N. B. Li, Copper induced phosphide for enhanced electrochemical hydrogen evolution reaction, Int. J. Hydrogen Energy 45 (2020) 21422-21430.
[27] C. Alexopoulou, A. Petala, Z. Frontistis, C. Drivas, S. Kennou, D.I. Kondarides, D. Mantzavinos, Copper phosphide and persulfate salt: a novel catalytic system for the degradation of aqueous phase micro-contaminants,

Appl. Catal. B Environ. 244 (2019) 178-187.
[28] S. Feng, B. Xiao, M. Wu, Y. Wang, R. Chen, H. Liu, Copper phosphide: a dual-catalysis-center catalyst for the efficient activation of peroxydisulfate and degradation of Orange II, Sep. Purif. Technol. 248 (2020) 117004.
[29] F. Rahmani, A. Ghadi, E. Doustkhah, S. Khaksar, In situ formation of copper phosphate on hydroxyapatite for wastewater treatment, Nanomaterials 12 (2022) 2650.
[30] L. Yan, B. Zhang, J. Zhu, S. Zhao, Y. Li, B. Zhang, J. Jiang, X. Ji, H. Zhang, P. K. Shen, Chestnut-like copper cobalt phosphide catalyst for all-pH hydrogen evolution reaction and alkaline water electrolysis, J. Mater. Chem. A 7 (2019) 14271-14279.
[31] M. Choi, S. Bong, J.W. Kim, J. Lee, Formation of 1-butanol from CO_2 without* CO dimerization on a phosphorus-rich copper cathode, ACS Energy Lett. 6 (2021) 2090-2095.
[32] H. Pfeiffer, F. Tancret, M.-P. Bichat, L. Monconduit, F. Favier, T. Brousse, Air stable copper phosphide (Cu_3P): a possible negative electrode material for lithium batteries, Electrochem. Commun. 6 (2004) 263-267.
[33] M.S. Chandrasekar, S. Mitra, Thin copper phosphide films as conversion anode for lithium-ion battery applications, Electrochim. Acta 92 (2013) 47-54.
[34] S. Licht, Aqueous solubilities, solubility products and standard oxidation-reduction potentials of the metal sulfides, J. Electrochem. Soc. 135 (1988) 2971.
[35] H. Kim, J. Lim, S. Lee, H.-H. Kim, C. Lee, J. Lee, W. Choi, Spontaneous generation of H_2O_2 and hydroxyl radical through O_2 reduction on copper phosphide under ambient aqueous condition, Environ. Sci. Technol. 53 (2019) 2918-2925.

[36] S. Wei, K. Qi, Z. Jin, J. Cao, W. Zheng, H. Chen, X. Cui, One-step synthesis of a self-supported copper phosphide nanobush for overall water splitting, ACS Omega 1 (2016) 1367-1373.
[37] S.-O. Kim, A. Manthiram, Phosphorus-rich CuP_2 embedded in carbon matrix as a high-performance anode for lithium-ion batteries, ACS Appl. Mater. Interfaces 9 (2017) 16221-16227.
[38] A. Manikandan, P. Sriram, K.-C. Hsu, Y.-C. Wang, C.-W. Chen, Y.-C. Shih, T.-J. Yen, H.-T. Jeng, H.-C. Kuo, Y.-L. Chueh, Electrochemically active novel amorphous carbon (a-C)/Cu_3P peapod nanowires by low-temperature chemical vapor phosphorization reaction as high efficient electrocatalysts for hydrogen evolution reaction, Electrochim. Acta 318 (2019) 374-383.
[39] R. Muruganantham, P.-C. Chiang, W.-R. Liu, Copper-diphosphide composites: a key factor evaluation and capacity enhancement route for high-energy lithium-ion storage, ACS Appl. Energy Mater. 1 (2018) 3674-3683.
[40] A. Rauf, M. Ma, S. Kim, S. Shah, C.-H. Chung, J. Park, P.J. Yoo, Mediator and co catalyst free direct Z-scheme composites of Bi_2WO_6-Cu_3P for solar-water splitting, Nanoscale 10 (2018) 3026-3036.
[41] W.R. Haag, J. Hoigne, Singlet oxygen in surface waters. 3. photochemical formation and steady-state concentrations in various types of waters, Environ. Sci. Technol. 20 (1986) 341–348.
[42] H. Cai, J. Zou, J. Lin, J. Li, Y. Huang, S. Zhang, B. Yuan, J. Ma, Sodium hydroxide-enhanced acetaminophen elimination in heat/peroxymonosulfate system:
production of singlet oxygen and hydroxyl radical, Chem. Eng. J. 429 (2022), 132438.
[43] G.-H. Moon, W. Kim, A.D. Bokare, N.-E. Sung, W. Choi, Solar

production of H_2O_2 on reduced graphene oxide-TiO_2 hybrid photocatalysts consisting of earth-abundant elements only, Energy Environ. Sci. 7 (2014) 4023-1028.

[44] A.A. Gorman, M.A.J. Rodgers, Singlet molecular oxygen, Chem. Soc. Rev. 10 (1981) 205–231.

[45] C. Schweitzer, R. Schmidt, Physical mechanisms of generation and deactivation of singlet oxygen, Chem. Rev. 103 (2003) 1685–1758.

[46] A. Schürmann, B. Luerßen, D. Mollenhauer, J. Janek, D. Schroder, Singlet oxygen in electrochemical cells: a critical review of literature and theory, Chem. Rev. 121 (2021) 12445–12464.

[47] F.E. Scully Jr., J. Hoign´e, Rate constants for reactions of singlet oxygen with phenols and other compounds in water, Chemosphere 16 (1987) 681-694.

논문개요

Copper phosphide (Cu_xP)는 특정 반응 조건(pH 3/dark)에서 자발적으로 hydroxyl radical을 생성하고 이를 통해 수중 오염물질을 분해하는 연구 결과가 발표된 바 있다. 그러나 산 조건에서는 Cu_xP의 용출 현상으로 인해 낮은 안정성을 갖는 단점이 있었으며, 중성 환경에서의 촉매 반응에 관한 연구는 보고된 바 없었다. 따라서, 본 연구에서는 중성 조건에서 반응의 안정성을 높이는 것을 목표로 하여 Cu_xP를 광촉매로 활용해 가시광선 조사하에 효과적인 거동을 확인했다. pH 3/ dark 조건에서는 산소와 과산화수소의 환원 과정에서 Cu, P 원소가 수용액으로 용출되며, 실험을 반복할수록 반응성이 점차 감소하는 경향을 보였다. 반면 pH 7에서 가시광선 조사 시에는 촉매의 안정성이 크게 향상돼 반복적인 오염물 분해 실험에도 분해 효율이 감소하지 않았다. 또한 각 반응 조건에 따라 달라지는 분해 반응 메커니즘을 규명했다. 두 시스템은 서로 다른 산화 메커니즘을 보였는데, 이는 각각의 시스템에서 생성되는 라디칼의 종류가 다르기 때문이다. 다양한 radical scavenger와 probe를 이용한 실험 결과, pH 3/dark에서는 전자전달 반응경로를 통해 산소를 환원시켜 과산화수소를 거쳐 강력한 산화력을 갖는 hydroxyl radical ($^{\bullet}OH$)이 생성되는 반면, pH 7/visible에서는 Cu_xP에서 시작한 에너지 전달 경로에 의해 singlet oxygen ($^1O_2$)이 생성되는 것을 확인했다. 이는 electron paramagnetic resonance (EPR) 분석으로 확실하게 증명했다. 이러한 Cu_xP 만의 특성은 선택적 산소 활성 종 생성을 통한 특정 유기 오염 물질 처리에 있어 새로운 전략과 고도 산화 공정 시스템 개발의 새로운 길을 제안한다.

주제어: 고도 산화 공정, Copper phosphide, Singlet oxygen, hydroxyl radical